IIETA International Information and Engineering Technology Association
Advancing the World of Information and Engineering

Journal Européen des Systèmes Automatisés
Vol. 59, No. 6, June, 2026, pp. 1573-1583
Journal homepage: http://iieta.org/journals/jesa

Essential Design Principles and Implementation Rules for Grid-Tied Inverters in Solar Energy Harvesting Systems

Salwan S. Sabry

Lecturer at the Sustainable Energy Engineering Department, University of Mosul, Mosul 41002, Iraq

Corresponding Author Email: salwan.samir@uomosul.edu.iq

https://doi.org/10.18280/jesa.590606

Received: 7 January 2026
Revised: 2 March 2026
Accepted: 23 March 2026
Available online: 30 June 2026

Keywords:
grid-connected inverter, perturb and observe, maximum power point tracking, three-phase voltage source inverter, synchronous reference frame, phase locked loop

ABSTRACT

This paper presents a complete and methodical design of a 25 kW photovoltaic (PV) system connected to the grid through a simple power conversion chain. The study begins with the modeling of the GESOLAR GES-P250 PV module, conventional DC-DC boost converter is employed to raise the PV output voltage to 800 V. The converter's duty cycle is regulated through a simple perturb and observe (P&O) maximum power point tracking (MPPT) algorithm. The output of the boost feeds a three-phase voltage source inverter (VSI) operated by classical sinusoidal pulse width modulation (SPWM). The inverter is synchronized with the grid through a reference synchronous frame (SF) phase locked loop (PLL), and its control system employs proportional integral (PI) regulators in both the inner current loop and the outer loop. The issue of grid-tied solar inverter is the lack of essential details to get a clear educational and technical guide for the design steps. Solar field harvesting contains multiple power converter stages to inject solar DC power to the grid utility efficiently. The goal of this work is to provide a clear understanding of these steps including control process and to eliminate ambiguities that are often found in related literatures. Every stage of the system, from the PV field, boost converter, and inverter, is derived and explained in detail, including the transformation from the (a,b,c) frame to the (α,β) and (d,q). The results show the system working perfectly by ensuring grid injected current's total harmonics distortion (THD) after the LCL filter at the point of common coupling (PCC) remains below the IEEE 519 limit of 5%. MATLAB Simulink is used to verify the stability and efficient performance of the proposed system. Simple disturbances for weather conditions changing the irradiance and temperature level for the solar field were applied to verify the responsibility of the proposed system. The target of this work is limited to the general design rules and control principles of grid-tied inverters under normal operating conditions for educational purposes. Advanced functions such as grid disturbance, overcurrent handling, and islanding detection are not considered for this study.

1. INTRODUCTION

In recent years, more solar power generation around the world has been substantially important in helping us reach the goal of net zero by 2050. Around the world, various renewable energy sources produce over 3.9 terawatt-hours (TWh) of energy annually. China constructed the largest solar photovoltaic (PV) systems in 2023. The most crucial factor for solar harnessing is technological development [1]. Figure 1 shows that the country also added more wind power and other resources. The figure demonstrates the historical and forecast solar PV capacity [2]. The solar system usually has multiple power conversions, such as a DC-DC stage to ensure that the field is tracking the optimal operating point and an inverter to interface the DC power to the grid or AC load. For the DC-DC converter, many researches had been introduced to offer optimal tracking algorithms for the field and regulate the DC output voltage. In the study [3], maximum power point tracking (MPPT) for the Cuk converter based on fuzzy logic control (FLC) is proposed. More proposed algorithms have been conducted, including incremental conductance (INC), particle swarm optimization (PSO), and the beta algorithm [4-6]. The inverter is the second part of the conversion in the solar system. There are two types of inverters: current source inverters (CSI) and voltage source inverter (VSI) [7, 8]. The VSI is usually used in grid-connected systems, while the CSI controls the output current waveforms by using an inductor to store energy. It is not used as much in PV systems, but it can be helpful in certain situations where current needs to be controlled [9]. VSIs are being used frequently in grid-connected PV systems because they can convert power in a way that is both flexible and effective. Some pulse width modulation (PWM) topologies used the idea of multilevel inverters (MLI), space vector pulse width modulation (SVPWM) [10, 11], model predictive control (MPC) [5], and even selective harmonics elimination (SHE) PWM to perform efficient inverter output waveforms by minimizing harmonic distortion. However, sinusoidal pulse width modulation

(SPWM) is still widely used in grid-connected inverters because it provides a good balance between simple implementation and acceptable.

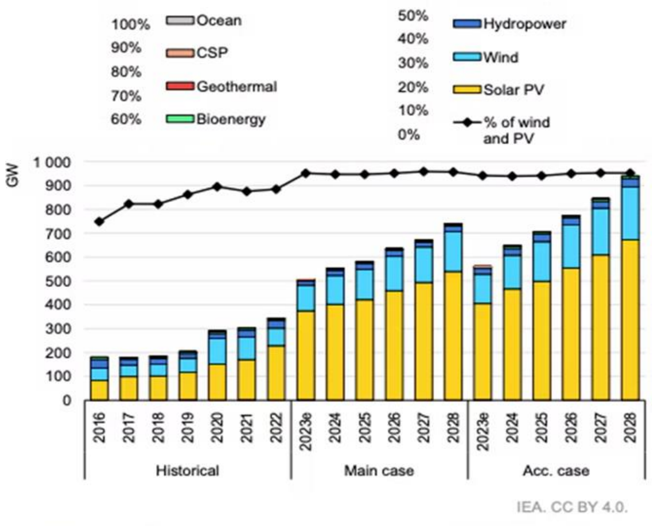

Figure 1. Renewable electricity capacity additions by technology and segment [2]

Note: CSP: concentrated solar power.

Table 1. Comparison of control approach for photovoltaic (PV) converter applications

Method Approach	Complexity	Time/ Sensing Needs	Applications
P&O + SPWM + PI	Low	Low	Small to medium scale, education
INC + SPWM + PI	Low/ moderate	Low/ moderate	The system needs better MPPT accuracy
(FLC/PSO) + MPC	High	High	Advanced optimization, research objective
FLC + SVPWM	Moderate/ high	Moderate/ high	Improving the inverter performance

Note: perturb and observe (P&O); sinusoidal pulse width modulation (SPWM); proportional integral (PI); incremental conductance (INC); fuzzy logic control (FLC); particle swarm optimization (PSO); model predictive control (MPC).

Harmonic performance, especially when an appropriate switching frequency and proper output filtering are applied. Grid-connected systems can dynamically balance supply and demand as part of a greater energy network to lower solar power intermittency [12]. A review of the aforementioned literature indicates that these topologies aren't simple to build and constructing a solar field. The problem formulation includes the utilization of using advanced MPPT and sophisticated PWM techniques, which add algorithmic complexity and multiple membership functions that are frequently challenging for practitioners and researchers to design while the proposed concept does not require FLC rule design, MLI, MPC, or computational overhead. Based on these studies, Table 1 summarises the comparison of control approaches for PV converters applications. The goal of the paper is to perform solar field grid integration via a simple perturb and observe (P&O) MPPT with a three-phase SPWM VSI. The proposed system offers a straightforward educational guideline for that purpose. The system's effectiveness will be demonstrated through a 25 kW simulation case study.

2. METHODOLOGY OF GRID-CONNECTED SOLAR FIELD

There would be three main steps to integrate a solar field with the utility grid. Firstly, starting with selecting proper PV modules to construct the field according to the power level required [13, 14]. Secondly, identifying the boost converter parameters according to the required power level and voltage [15, 16]. Lastly, the appropriate inverter specifications are selected for grid interfacing [12].

2.1 Selecting photovoltaic module

The PV module has key definitions that can be found in its datasheet, usually at standard test conditions (STC) such as irradiance (1000 W/m²), temperature (25 ℃), and air mass (AM) (1.5 standardised spectrum of light that accounts for the path the sunlight takes through the Earth's atmosphere). The essential PV module parameters can be demonstrated as below [17, 18]:

- $P_{Max,\ TC}$: Maximum panel power rating at STC (W).
- $V_{OC,\ STC}$: Open circuit voltage at STC (V).
- $I_{SC,\ STC}$: Short circuit current at STC (A).
- $V_{MPP,\ STC}$: Voltage at maximum power point (MPP) and STC (V).
- $I_{MPP,\ STC}$: Current at MPP and STC (A).

According to IEC 61215 [13], building a PV array needs a number of series/parallel combinations of PV modules.

$$P_{Max,STC} = V_{MPP,STC} \times I_{MPP,STC}\ (W) \tag{1}$$

The string voltage at MPP and STC would be:

$$V_{Str,MPP} = N_S \times V_{MPP,STC}\ (V) \tag{2}$$

where,

N_S: the number of series modules per string.

The string current at MPP and STC would be:

$$I_{Str,MPP} = I_{MPP,STC}\ (A) \tag{3}$$

The array voltage at MPP would be:

$$V_{Array,MPP} = N_S \times V_{MPP,STC}\ (V) \tag{4}$$

The array current at MPP would be:

$$I_{Array,MPP} = N_P \times I_{MPP,STC}\ (A) \tag{5}$$

where,

N_P: the number of parallel strings.

The array power at STC condition is given by Eq. (6).

$$P_{Array,STC} = V_{Array,MPP} \times I_{Array,MPP} = N_S \times V_{MPP,STC} \times N_P \times I_{MPP,STC} = N_S \times N_P \times P_{MPP,STC}\ (W) \tag{6}$$

This equation is significant for identifying the number of series panels and parallel strings.

$$N_S \times N_P = \frac{Power\ (PV\ field)}{P_{MPP,STC}} \tag{7}$$

2.2 Boost converter specifications

The boost converter functions two main goals in this system. The first one is to elevate the input voltage up to a certain value that would fit the inverter input side, while the second function is to achieve the MPP operating for the solar field. Assuming the boost converter is working in continuous conduction mode (CCM). According to the inductor volt-second balance principle, during the on-interval (D = 1) the inductor voltage is equal to the source voltage, while during the off-interval (D = 0) the inductor voltage is equal to the difference between the input voltage source and the load voltage. As a result, the boost converter output voltage is explained by the following equations [15].

$$V_{Out} = \frac{V_{in}}{1-D}\ (V) \tag{8}$$

D is the duty ratio of the boost converter. V_{in}, V_{Out} are the converter input and output voltages, respectively. The converter average input current would be as follows [16]:

$$I_{in,Boost,Ave} = \frac{Power}{V_{in}}\ (A) \tag{9}$$

For 5% current ripple

$$\triangle I_L = I_{in,Boost,Ave} \times 0.05\ (A) \tag{10}$$

For CCM, the value of L would be [16]:

$$L \geq \frac{V_{in} \times D}{\triangle I_L \times f_{SW}}\ (H) \tag{11}$$

f_{SW} is the switching frequency for the converter. L is the converter's inductor. To size the boost converter output capacitor C_{Out} for a certain allowable voltage ripple $\triangle V_{Out}$ (5%), neglecting the ESR, Eq. (12) can be used [16].

$$\triangle V_{Out} \approx \frac{I_{Out} \times D}{C_{Out} \times f_{SW}} \qquad C_{Out} \geq \frac{I_{Out} \times D}{\triangle V_{Out} \times f_{SW}}\ (F) \tag{12}$$

Table 2. Scheme of the conventional perturb and observe (P&O) maximum power point tracking (MPPT) algorithm [22]

Sign of ΔP	Sign of ΔV	Resulting Perturbation
Positive	Positive	+ve
Positive	Negative	-ve
Negative	Positive	-ve
Negative	Negative	+ve

To keep the PV field operating near the MPPT, multiple algorithms can be utilized. Some of these algorithms add a sort of complexity, delaying the time for computation due to their advanced approaches [19, 20]. The study [19], it presents a variable step-size P&O algorithm augmented with FLC to enhance dynamic response and tracking precision in a grid-connected PV system. In the study [20], the proposed idea was to integrate Takagi-Sugeno fuzzy modeling with an Adaptive Neuro-Fuzzy Inference System (ANFIS) predictor to manage partial shading. This hybrid approach gets high accuracy and good response, but it needs multi-stage modeling, Lyapunov stability analysis, and tuning based on convex optimization. These advanced approaches may add complexity for beginner engineers to use or understand these concepts. In contrast, simple P&O MPPT combined with a boost converter provides a clear roadmap for designers. It focuses on making things clear and possible in real time. Table 2 explains the P&O scheme to track the MPPT for a PV field [21, 22]. Voltage and current for the field have to be measured. According to the change in voltage ΔV and power ΔP, the algorithm will make the decision by changing the D for the boost converter.

2.3 Three-phase inverter specifications

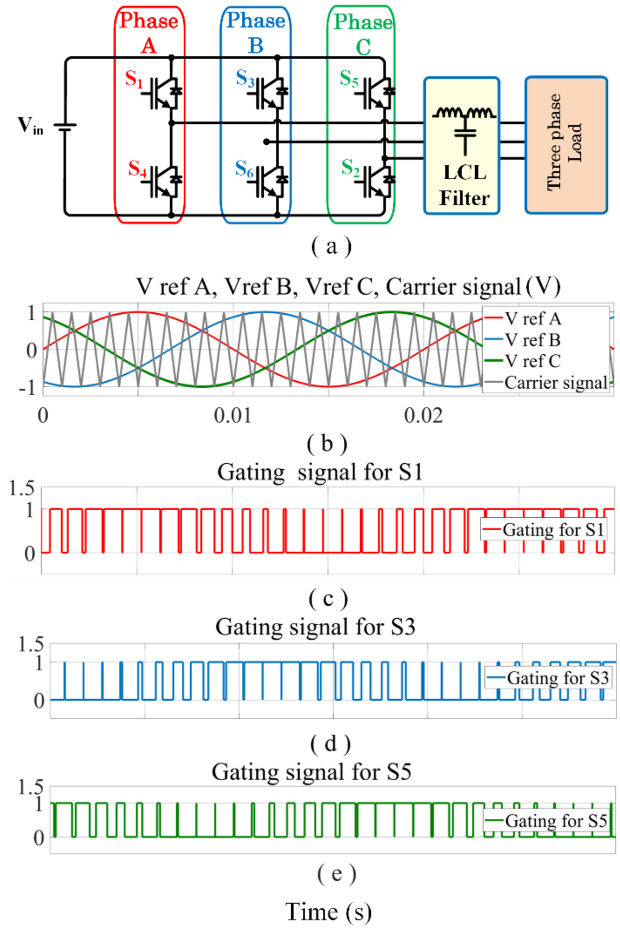

Figure 2. Three phase voltage source inverter (VSI) (a) main circuit diagram with the presence of a DC source and an LCL filter, (b) three phase reference voltages signals (V ref A, V ref B, V ref C) with high frequency carrier signal, (c) gating signal for switch S_1, (d) gating signal for S_3, (e) gating signal for S_5

This section will discuss the principal operations of three-phase VSI. For the SPWM technique, grid interfacing inverter with proportional integral (PI) control structure in the synchronous frame (SF) will be covered. Lastly, an LCL filter design will be discussed. Firstly, the operating principles for the SPWM are demonstrated in Figure 2. Solar inverters utilize PWM techniques to create efficient inverter output waveforms. The most commonly used technique is the regular SPWM, as illustrated in Figure 2. This figure shows the main circuit diagram of a three-phase VSI with the presence of a DC source and an LCL filter. It demonstrates the getting signals for each phase by comparing the reference signals V ref A, V ref B, V ref C, with a high frequency carrier signal to get the gating signal (S1, S3, and S5). Gating signal for (S4, S6, and S2) would be the flipped version of forementioned signals respectively. Inverter designers find that the SPWM is perfect choice since it is easy to build and control. The modulation index (m_a) is defined as the ratio of the peak amplitude of the reference signal to the peak amplitude of the high-frequency carrier signal (usually a triangular wave) in the SPWM technique, as illustrated in Figure 2 and given in Eq. (13) [23, 24].

$$m_a = \frac{Vref\ ,Peak}{VCarrier,Peak} \tag{13}$$

To prevent the output waveform from exceeding the system's voltage rating, this m_a is normally restricted to a value of one ($m_a \leq 1$) for standard SPWM. For the three-phase VSI utilizing the SPWM, the fundamental output voltage depends on the DC bus voltage and m_a. The peak phase voltage would be [23]:

$$V_{ph,peak} = \frac{m_a \times V_{dc}}{2} \tag{14}$$

The fundamental root mean square voltage (RMS) line to line voltage would be [23]:

$$V_{ll,RMS} = \frac{\sqrt{3}}{2\times\sqrt{2}} \times m_a \times V_{dc} \tag{15}$$

Thus, selecting 800 V DC bus voltage allows the inverter to produce around 400 V while maintaning the m_a under the unity value. The SHE PWM is a sophisticated technique designed to minimize specific harmonic components in the output waveform. By selecting and eliminating some low-order harmonics, this method improves the output voltage quality and reduces the need for complicated filtering. However, this modulation is not recommended for variable operating points [25]. Secondly, the inverter and grid have to have the same voltage sequence and frequency [26, 27]. The phase locked loop (PLL) can be used to accomplish this rule [28, 29]. The PLL's primary job is to determine the grid frequency so that the inverter synchronizes with the grid. The grid's voltages and the inverter's currents should be transformed from the (a, b, c) frame to the SF (d, q, 0) with a grid angle θg from the PLL and rotate (Alpha, Beta, 0) into an SF to construct a PI controller for the grid-connected inverter [30, 31]. Figure 3 demonstrates the PI structure for the grid-connected inverter. Starting by converting the voltages/currents from a three-phase system (variable with time) to a two-phase system (Alpha, Beta) using Clark transformation and then to direct & quadrature (d, q, 0) components using Park transformation, which is given by the following equations [32, 33]:

$$\begin{bmatrix} f_\alpha \\ f_\beta \end{bmatrix} = \sqrt{\frac{2}{3}} \times \begin{bmatrix} 1 & -\frac{1}{2} & -\frac{1}{2} \\ 0 & \frac{\sqrt{3}}{2} & -\frac{\sqrt{3}}{2} \end{bmatrix} \times \begin{bmatrix} f_a \\ f_b \\ f_c \end{bmatrix} \tag{16}$$

$$\begin{bmatrix} f_d \\ f_q \end{bmatrix} = \begin{bmatrix} \cos(\theta g) & \sin(\theta g) \\ -\sin(\theta g) & \cos(\theta g) \end{bmatrix} \times \begin{bmatrix} f_\alpha \\ f_\beta \end{bmatrix} \tag{17}$$

θg: is the grid voltage angle.

PI controllers perform better when controlling variables that remain nearly constant in the selected RF. The Clarke and Park transformations are used to convert three-phase, time varying AC quantities into DC like variables within a rotating reference SF. This transformation simplifies the control process because, under steady state conditions, the controlled variables become nearly constant. The Figure demonstrates this transformation process with the PI controller. The overall outcome of this process would be the Vref A, Vref B, Vref C. To suppress the high-order harmonics further for the inverter output currents, an LCL filter could be utilized between the inverter and the grid. To avoid the interaction with the control system, the filter resonance frequency (f_{res}) should be chosen carefully. Commonly design guideline to choose the f_{res} is given in Eq. (18) [34].

$$10 f_{grid} < f_{res} < \frac{f_{sw}}{2} \tag{18}$$

f_{grid}: the grid frequency (Hz).
f_{res}: the LCL filter resonance frequency (Hz).
f_{SW}: the inverter switching frequency (Hz).

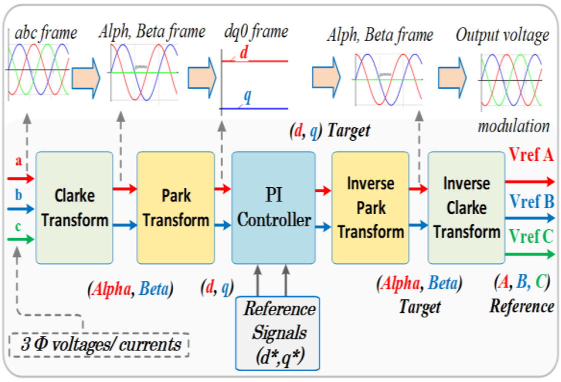

Figure 3. Synchronous frame (SF) transformations with the proportional integral (PI) controller structure for grid-connected inverter

To evaluate the LCL filter value per phase, Eq. (19) can be used [34, 35].

$$\omega_{res} = \sqrt{\frac{L_1 + L_2}{L_1 . L_2 . C}} \tag{19}$$

ω_{res} is the resonance angular frequency (rad/sec). C is the filter's capacitor (F).

For ($L_1 = L_2 = 500$ μH, C = 200 μF), $\omega_{res} \approx 4472$ rad/sec.

In order to suppress the oscillation further, a passive damping resistor (R_d) is connected in series with the filter's capacitor.

The approximate value of R_d is given by Eq. (20) [35].

$$R_d \approx \frac{1}{3.\omega_{res}.C} \approx 0.37\Omega \tag{20}$$

The purpose of the LCL filter to smooth the grid injected current at the point of common coupling (PCC) to stay with the limit of IEEE 519 [36].

3. PROPOSED DESIGN EXAMPLE FOR SOLAR FIELD GRID-CONNECTED

3.1 General design rules for grid-connected inverter

According to the methodology discussed in the previous sections, several general design rules can be identified as follows:

- DC bus voltage selection rule.
- Control bandwidth rule.
- LCL filter resonance rule.
- THD evaluation at the PCC rule.

3.2 Design rules for the 25 kW case study

Figure 4 demonstrates the three main steps for a grid-connected solar field, starting with selecting a PV module, identifying boost converter parameters, and specifying inverter parameters. Figure 5 shows the overall proposed circuit diagram for the solar grid integration. Demonstrating the 25 kW solar field, DC-DC boost converter, and three-phase VSI. Table 3 demonstrates the proposed circuit parameters, including the PI controller's gains (KP, KI), LCL filter, and the grid parameters. These gains were primarily tuned through simulation-based refinement and verified to achieve stable response of current-loop with bandwidth. The structure of PI controller in the SF is detailed using the following steps:

Step 1: Transfer the three-phase voltages/currents from (a, b, c) frame to the (d, q) frame using Eqs. (16) and (17).

Step 2: To ensure the inverter is synchronized with the grid, PLL can be used.

Step 3: To control the real power (P), reactive power (Q), Eqs. (21) and (22) demonstrate the instantaneous power in the SF [33].

$$p = \frac{3}{2}(V_d \times I_d + V_q \times I_q)\ (W) \tag{21}$$

$$Q = \frac{3}{2}(V_q \times I_d - V_d \times I_q)\ (VAR) \tag{22}$$

In the reference SF, i_d represents P while i_q represents Q. For this case, i_q set to be zero, which means unity power factor at the PCC under balanced grid conditions.

Step 4: To formulate the dynamic response in the SF for a simple RL circuit, the following equations can be used [34].

$$V_d = R.I_d + L.\frac{di_d}{dt} - \omega.L.i_q\ (V) \tag{23}$$

$$V_q = R.I_q + L.\frac{di_q}{dt} + \omega.L.i_d\ (V) \tag{24}$$

V_d, V_q/ i_d, i_q are the voltages/current in the SF respectively. R, L are the resistance in Ω and inductance in H between the inverter and the grid, respectively. ω is the angular frequency usually it is the grid frequency in (rad/ second). To ensure the PV field is working at the MPPT, the P&O algorithm can be used as explained in Figure 6. This algorithm operates as hysteresis control by oscillating around the MPP. It depends on the △P and △V to obtain the decision, which is increasing or decreasing the PV field voltage by changing the D of the boost converter as explained in Figure 7. The complete control structure of the proposed grid-connected inverter is illustrated in Figures 3 and 5, which involve the reference SF transformations, PI current control loops, and PWM modulation stage. For grid-connected inverter, to ensure good current tracking, the inner current control loop should be operated faster than the outer control loop. For inverter switching frequency of 15 kHz, the current loop bandwidth is selected 10% of the switching frequency. Thus, the current controller bandwidth in this work is about 1 to 1.5 kHz. The PLL used in grid synchronization operates with a much lower bandwidth to avoid interaction with the current control loop. Typical PLL bandwidth values are between 50 to 100 Hz, to ensure stable grid synchronization, which is demonstrated in the results and validations section.

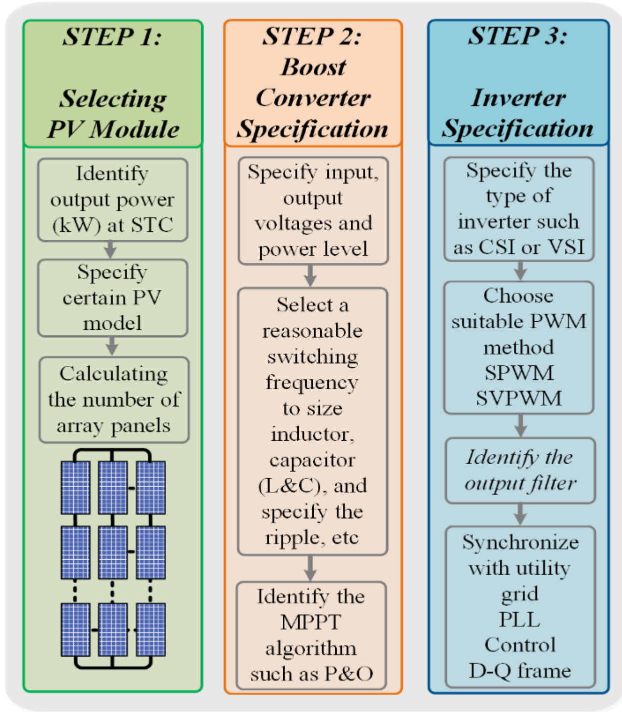

Figure 4. Main steps for solar field grid-connected system

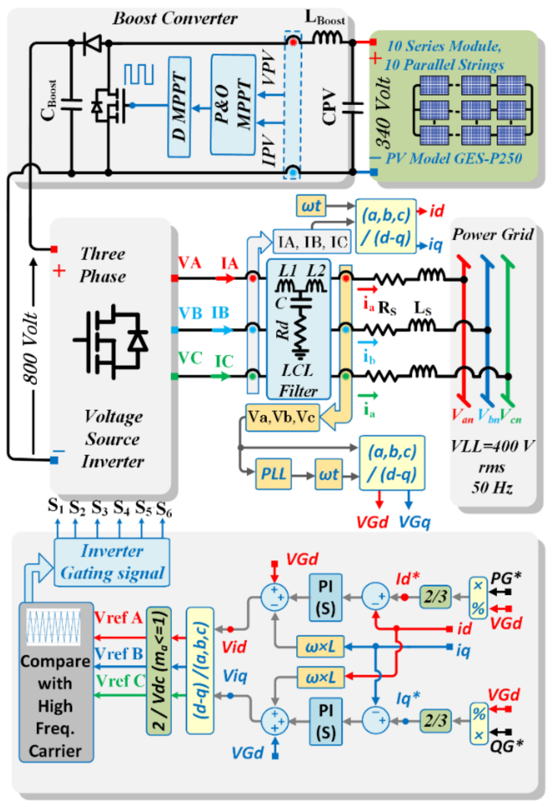

Figure 5. Proposed grid-connected system configuration: a 25 kW solar field with DC-DC boost converter, three-phase voltage source inverter (VSI), and proportional-integral (PI) controller in the synchronous frame (SF)

Table 3. Circuit parameters for the proposed shown in Figure 5

PV Field Specifications	**Panel Model: GES-P250**	**N_S: 10 N_P: 10**	**Vpv = 340 V, CPV = 2 mF**	**$P_{MAX, STC}$ = 25 kW**
Boost converter specifications	Vin = 340 V Vout = 800 V	L_{Boost} = 0.085 mH C_{Boost} = 600 µF		Switching frequency 10 kHz
Inverter specifications	Type VSI	$L_1 = L_2$ = 500 µH C_{Filter} = 200 µF Rd = 0.37 Ω		Switching frequency 15 kHz
PI controller Gains	KP ≈ 4.7 Ki ≈ 4800	Tuned through simulation-based for better performance		
Grid utility specifications	Ls = 20 µH, Rs = 10 mΩ	$V_{ll, RMS}$ = 400 V 50 Hz		Y connected

Note: photovoltaic (PV); GESOLAR Photovoltaic module, 250W, (GES-P250); Number of series modules per string (N_S); Number of parallel strings (N_P); Photovoltaic field total voltage (Vpv); Capacitor across photovoltaic field (CPV); Maximum solar field power rating at standard test conditions ($P_{MAX,STC}$); Inductor for the boost converter (L_{Boost}); Capacitor for the boost converter (C_{Boost}); Voltage source inverter (VSI); LCL filter inductor (L_1,L_2); LCL filter capacitor (C_{Filter}); LCL filter passive damping resistor (Rd); Proportional gain (KP); Integral gain (KI); Grid Source inductance (L_S); Grid source resistance (R_S); Line to line root mean square voltage (V_{llRMS}); Wye or star connected for the grid utility (Y).

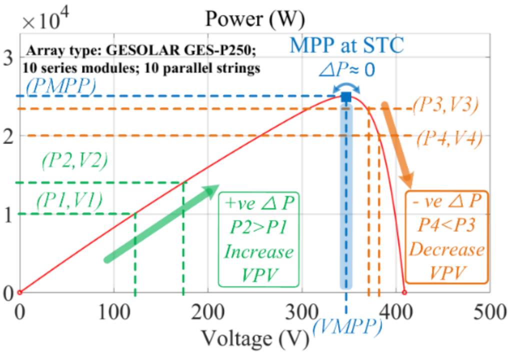

Figure 6. Perturb and observe (P&O) maximum power point tracking (MPPT) algorithm

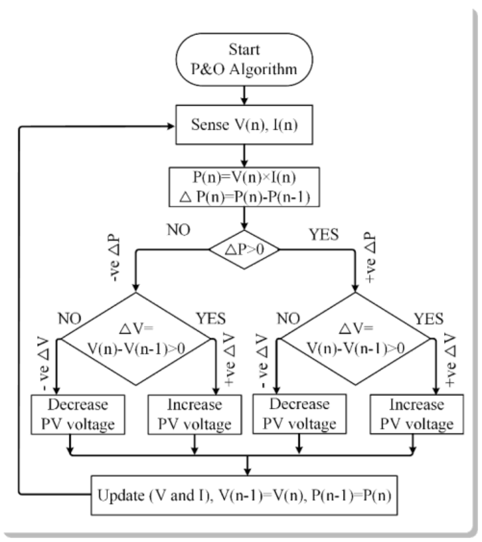

Figure 7. Flowchart for the perturb and observe (P&O) maximum power point tracking (MPPT) algorithm

4. RESULTS AND VALIDATIONS

Table 4. MATLAB simulation setup parameters

Sover Type Ode23t (mod.stff/ Trapezoidal)	**Step Size 1 µ Sec**	**Control Sampling Time Ts = 10 µ Sec**
THD Analysis time window (0.65-0.85) sec	Fundamental frequency for the FFT 50 Hz	Number of cycles 10
Inverter Semiconductor switch IGBT/Diode Ron 1 mΩ	Boost converter Semiconduct Diode Ron 1 mΩ	Boost converter Diode forward voltage 0.8 V

The presented solar inverter was modeled in MATLAB/Simulink to verify the design procedure and control performance. The simulation includes the PV field, boost converter, VSI, reference SF, PLL, PI current controllers, and LCL filter. The main operating conditions and analysis settings are summarized in Table 4. The results contain three sections: PV solar field, DC-DC boost converter, and inverter. Firstly, for the solar field, Figures 8 and 9 illustrate the characteristics of the 25 kW solar field. These figures demonstrate the IV and PV profiles for three irradiance levels (500, 750, and 1000) W/m^2 and three temperature values (25, 35, and 45) °C respectively. It indicates that the operating field's voltage is approximately 340 volts and the available power reaches 25 kW for standard operating condition. Secondly, for the boost converter results, Figure 10 illustrates the input/output converter voltages along with the converter PWM pulses. The boost converter functions to track the MPP (utilizing the P&O algorithm) for the PV field and elevate the output voltage up to 800 V.

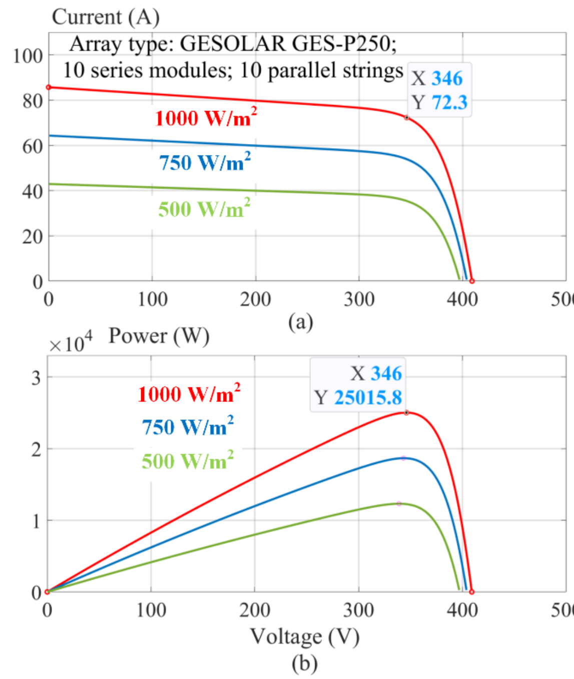

Figure 8. 25 kW solar field characteristic for three irradiance levels (500, 750, 1000) W/m^2 that contains 10 Panels in series and 10 parallel strings, photovoltaic (PV) module GES-P250 (a) IV characteristics, (b) PV characteristics

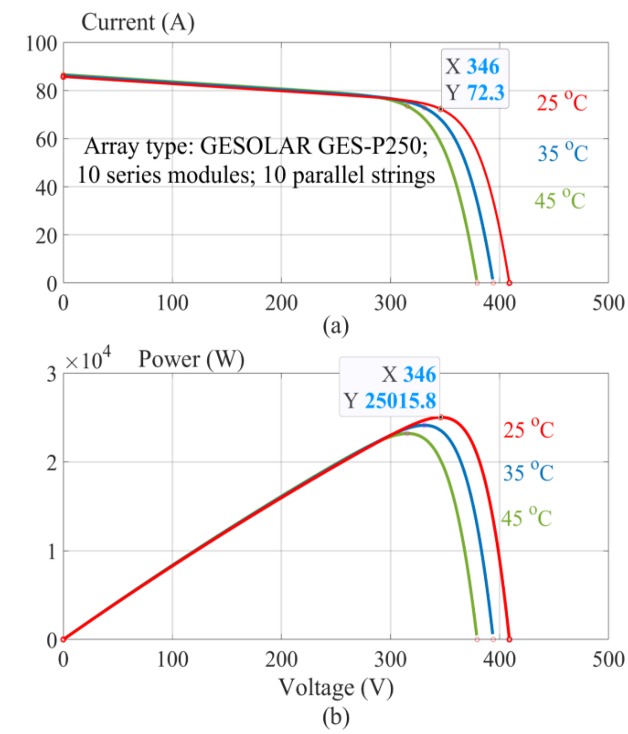

Figure 9. 25 kW solar field characteristic for three temperature values (25, 35, 45) °C that contains 10 Panels in series and 10 parallel strings, photovoltaic (PV) module GES-P250 (a) IV characteristics, (b) PV characteristics

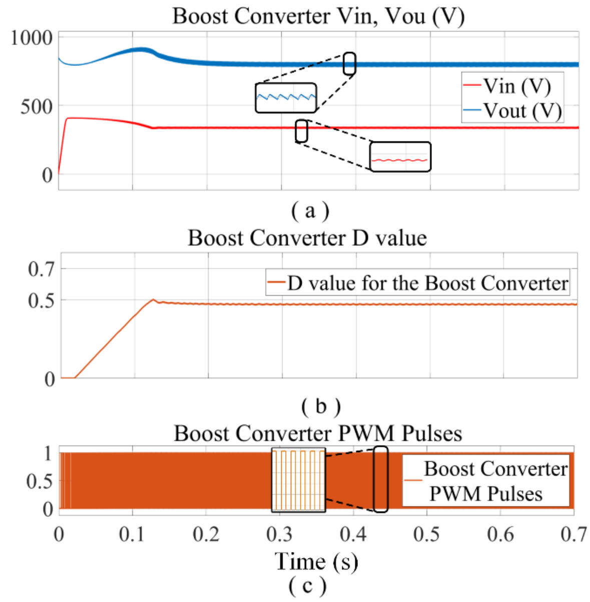

Figure 10. Boost converter results (a) input/output voltages, (b) duty ratio (D) value obtains by the perturb and observe (P&O), (c) pulse width modulation (PWM) pulses for the converter

Lastly, for the inverter results, Figure 11 demonstrates the transformation process from the (a, b, c) frames to the (d,q) frame. It shows the grid voltages, PLL signal, (Alpha-Beta) frame, and (d,q) frame. The PLL output signal varies between (0 to 2π) illustrating the estimated grid phase angle. The figure shows the waveform period in the simulation is 20 ms for 50 Hz grid frequency, confirming the synchronization between the inverter and the grid. Figure 12 demonstrates the output of the PI controller, which is the (Vref A, Vref B, and Vref C) for the inverter PWM along with the high-frequency carrier signal (15 kHz). Additionally, the gating signals for phase A (S1, S4) are illustrated. Similarly, the gating signals for phases B and C would be shifted by 1200. To maintain (ma ≤ 1), the output of the PI controller would be multiplied with (2/Vdc) as shown in Figure 5 and given by Eq. (14). Figure 13 shows the inverter's output voltages (VA, VB, and VC) along with their currents (IA, IB, and IC) before the LCL filter (inverter bridge currents). Moreover, the inverter bridge current IA's THD is approximately 10%. For the grid-side results, the proposed system was tested for two weather disturbance conditions to evaluate the system stability. Starting to vary the irradiance level and changing the temperature condition for the solar field.

To vary the irradiance levels, Figure 14 shows the grid voltages (Va, Vb, and Vc) along with the grid-injected current (ia, ib, and ic) after the LCL filter at the PCC. The irradiance level was changed from 1000 to 500 W/m^2 for that disturbance. The figure demonstrates that the injected grid power is aligned with the irradiance level and available solar field DC power. Furthermore, the THD for the inverter output current IA (prior to the LCL filter) and grid-injected current ia (after the LCL filter) are depicted, demonstrating that ia is within the acceptable limit of less than 5% for the steady-state condition, demonstrating the LCL filter's good performance. The second disturbance was changing the solar field's temperature profile (25, 45, 25) °C. In response to the change in temperature, Figure 15 shows the results.

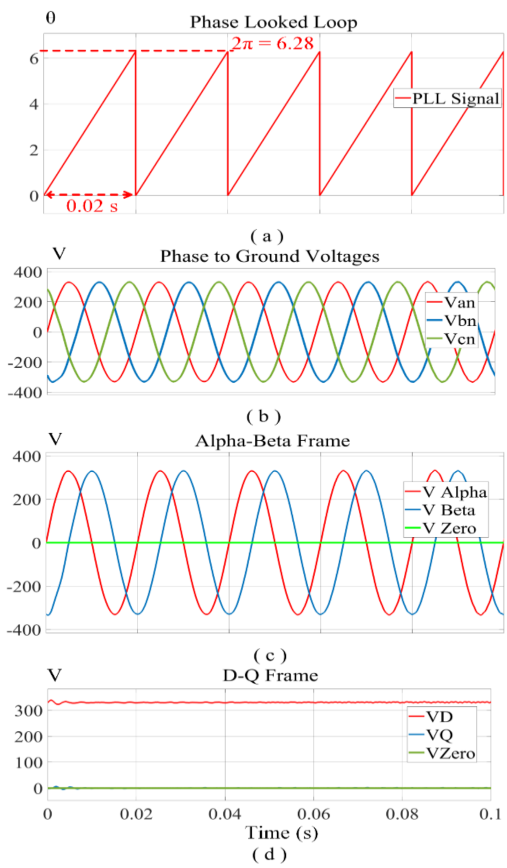

Figure 11. Transformation from (a,b,c) frame to (d,q) frame (a) phase locked loop (PLL) signal confirming the synchronization between the inverter and grid (b) grid voltages (Van, Vbn, Vcn), (c) (V Alpha, V Beta, V Zero), (d) d,q frame (VD, VQ, VZero)

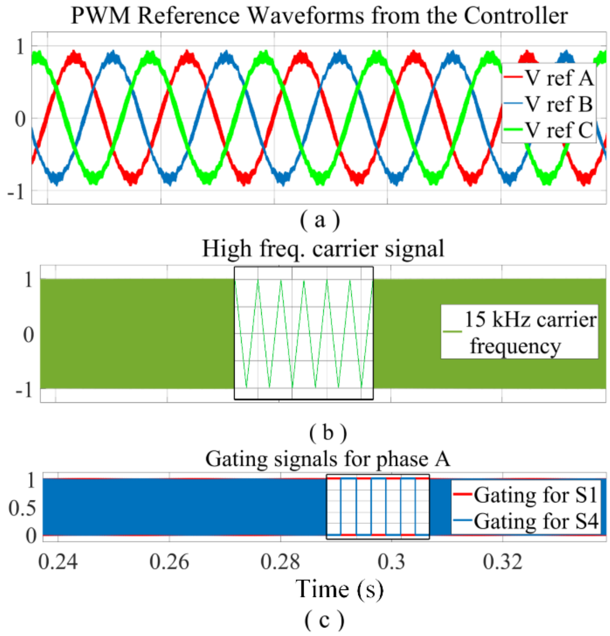

Figure 12. The proportional integral (PI) controller results and pulse width modulation (PWM) signals (a) inverter reference waveforms (V ref A, V ref B, V ref C), (b) high frequency 15 kHz carrier signal, (c) gating signals for phase A (S1, S4)

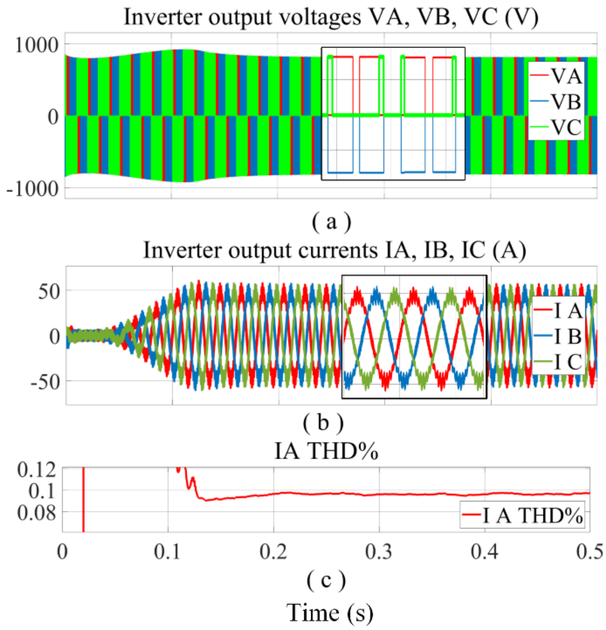

Figure 13. Inverter output results (a) inverter output voltages (VA, VB, VC), (b) inverter output current (IA, IB, IC), (c) total harmonics distortion (THD) for the phase A current IA before the LCL filter

The steady state THD analysis for the bridge inverter current IA prior to the LCL filter and the grid-injected current ia after the LCL filter at the PCC are shown in Figures 16 and 17, respectively. They were calculated during steady state condition with time window between 0.65 to 0.85 seconds as illustrated in the figures. They were measured after irradiance level get back to 1000 W/m^2. The fundamental frequency is 50 Hz and the sampling rate based on the simulation time is 1e-6.

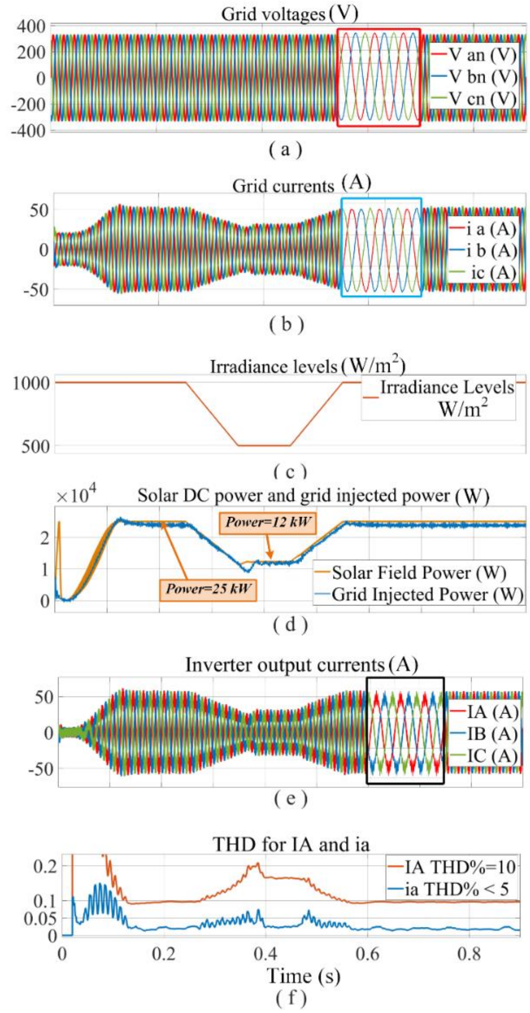

Figure 14. Results for varying the irradiance levels (1000 to 500) W/m^2 (a) grid voltages (Van, Vbn, Vcn), (b) grid injected currents (ia, ib, ic) after the LCL filter, (c) irradiance levels, (d) solar power levels along with the injected power to the grid, (e) inverter bridge currents (IA, IB, IC) before the LCL filter, (f) total harmonics distortion (THD) for the inverter output current IA before the LCL filter and the injected grid current iA after the LCL filter

5. CONCLUSION

This paper offered a complete pathway to design, model, and control a 25 kW solar field that can be integrated with the grid utility in a stable and reliable way. Starting with selecting the proper PV module GES-P250 from the MATLAB library. Additionally, the paper provided a detailed explanation and development of DC-DC boost converters, inverter modulation, and grid synchronization. Furthermore, a simple classic PI controller was designed and explained in the SF. The use of simple, traditional methods such as P&O MPPT, SPWM, and classic PI control demonstrates essential simplicity, which can often lead to increased reliability, clarity, and educational value. The simulation results show that the proposed solar field can harvest the solar power and inject clean current at the PCC after the LCL filter into the grid with a THD (< 5%) that is below IEEE 519 limits. The real value of this research is offering a road map teaching tool by integrating theoretical and technical aspects into a clear framework, enabling the development of a solar field grid integration system. The paper makes a complicated system easier to understand by breaking down each control and transformation step. This makes it a useful and understandable example of sustainable energy engineering. It is both a technical contribution and a learning tool that helps engineers work toward the bigger goal of reliable solar grid injected energy conversion. This study is intended to provide good framework for explaining the general design rules of grid-tied inverters under normal operating conditions. Therefore, advanced grid-support and protection functions, were not considered in the present study.

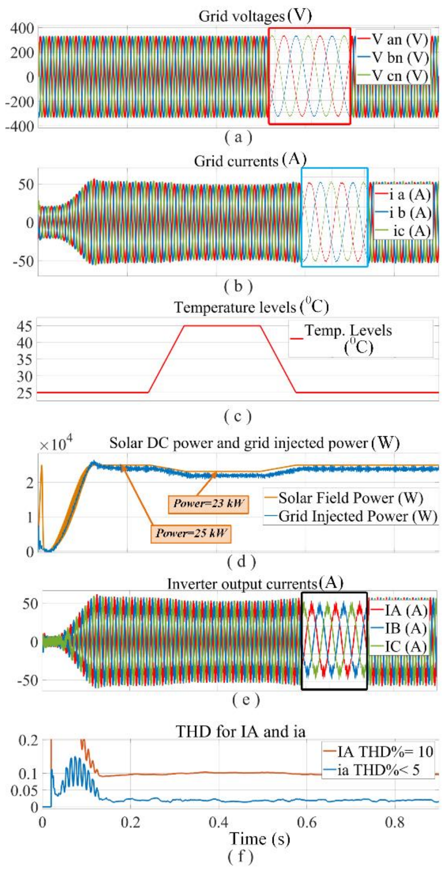

Figure 15. Results for varying the temperature values (25, 35, 45) °C (a) grid voltages (Van, Vbn, Vcn), (b) grid injected currents (ia, ib, ic) after the LCL filter, (c) temperature profile, (d) solar power levels along with the injected power to the grid, (e) inverter output currents (IA, IB, IC) before the LCL filter, (f) total harmonics distortion (THD) for the inverter output current IA before the LCL filter and the injected grid current iA after the LCL filter

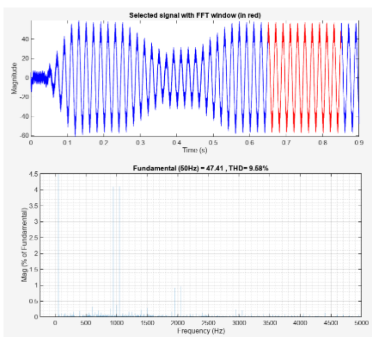

Figure 16. Total harmonics distortion (THD) analysis at steady state condition for the inverter bridge current iA before the LCL filter

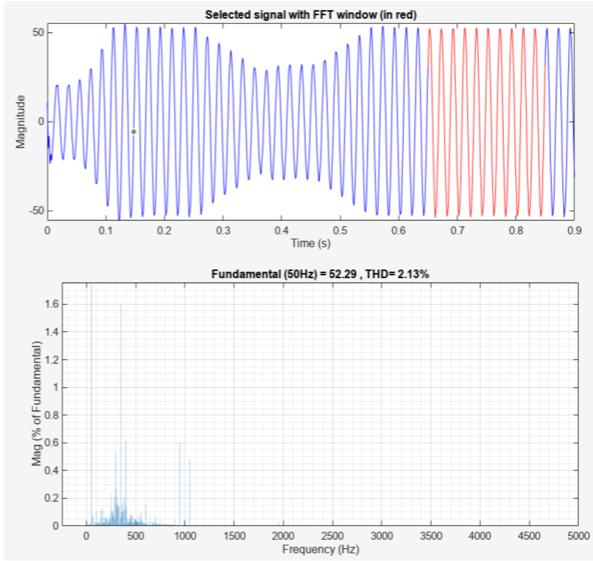

Figure 17. Total harmonics distortion (THD) analysis at steady state condition for the grid-injected current iA after the LCL filter

ACKNOWLEDGMENT

The author would like to thank the University of Mosul, Iraq, for its support during this research.

REFERENCES

[1] Al-Greer, M., Chowdhury, R., Sajeevan, A., Sabry, S., Suhail, A., Abdulwahid, O. (2024). Solar energy education: Curriculum framework development. In Proceedings of the IEEE International Symposium on Systems Engineering, Perugia, Italy, pp. 1-6. https://doi.org/10.1109/ISSE63315.2024.10741109

[2] Wood, J. (2024). The world added 50% more renewable capacity last year than in 2022. World Economic Forum. https://www.weforum.org/stories/2024/02/renewables-energy-capacity-demand-growth/, accessed on May 2025.

[3] Themozhi, G., Srinivasan, K., Srinivas, T., Prabha, A. (2024). Analysis of suitable converter for the implementation of drive system in solar photovoltaic panels. Electrical Engineering & Electromechanics, (1): 17-22. https://doi.org/10.20998/2074-272X.2024.1.03

[4] Bhavani, M., Reddy, K., Mahesh, K., Saravanan, S. (2023). Impact of variation of solar irradiance and temperature on the inverter output for grid connected photovoltaic systems at different climate conditions. Materials Today: Proceedings, 80: 2101-2108. https://doi.org/10.1016/j.matpr.2021.06.120

[5] Zhao, Y., An, A., Xu, Y., Wang, Q., Wang, M. (2021). Model predictive control of grid-connected PV power generation system considering optimal MPPT control of PV modules. Protection and Control of Modern Power Systems, 6(1): 32. https://doi.org/10.1186/s41601-021-00210-1

[6] Jabbar, R., Mekhilef, S., Mubin, M., Mohammed, K. (2023). A modified perturb and observe MPPT for a fast and accurate tracking of MPP under varying weather conditions. IEEE Access, 11: 76166-76176.

https://doi.org/10.1109/ACCESS.2023.3297445
[7] Sabry, S., Pool-Mazun, E., Enjeti, P. (2019). A medium voltage DC collection grid for large scale PV power plant with SCR converter and integrated solid-state transformer. In Proceedings of the IEEE Energy Conversion Congress and Exposition (ECCE), Baltimore, USA, pp. 5824-5831. https://doi.org/10.1109/ECCE.2019.8913251
[8] Sabry, S., Alsammak, A. (2024). Power density enhancement of three-phase rectifier using higher frequency solid state transformer. Mathematical Modelling of Engineering Problems, 11(5): 1286-1292. https://doi.org/10.18280/mmep.110518
[9] Hamid, S., Alsammak, A., Atta, K. (2023). Using solar photovoltaic systems, battery energy storage systems and underfrequency load shedding to improve frequency stability of power systems. Al-Rafidain Engineering Journal, 28(1): 165-172. https://doi.org/10.33899/rengj.2022.136061.1201
[10] Alrawe, M., Husien, M. (2023). A comparative study of total harmonic distortion between two topologies 27- and 31-level multilevel inverter. Al-Rafidain Engineering Journal, 28(1): 173-180. https://doi.org/10.33899/rengj.2022.134999.1192
[11] Parimalasundar, E., Kumar, N., Geetha, P., Suresh, K. (2022). Performance investigation of modular multilevel inverter topologies for photovoltaic applications with minimal switches. Electrical Engineering & Electromechanics, (6): 28-34. https://doi.org/10.20998/2074-272X.2022.6.05
[12] Yu, Y. (2024). Comparison of three-phase inverter modulation techniques: A comprehensive analysis of SPWM and SVPWM. Highlights in Science, Engineering and Technology, 97: 185-196. https://doi.org/10.54097/q80q3f10
[13] International Electrotechnical Commission, IEC 61215-1:2021, Terrestrial Photovoltaic (PV) Modules Design Qualification and Type Approval Feb. 2021. https://webstore.ansi.org/preview-pages/IEC/preview_iec61215-1%7Bed2.0%7Db.pdf.
[14] Alkahtani, M., Kamari, N., Zainuri, M., Syam, F. (2024). Design of grid-connected solar PV power plant in Riyadh using PVsyst. Energies, 17(24): 6229. https://doi.org/10.3390/en17246229
[15] Raiker, A., Loganathan, U., Reddy, S. (2021). Current control of boost converter for PV interface with momentum-based perturb and observe MPPT. IEEE Transactions on Industry Applications, 57(4): 4071-4079. https://doi.org/10.1109/TIA.2021.3081519
[16] Hauke, B. (2022). Basic calculation of a boost converter's power stage. Texas Instruments Application Note SLVA372D. Available: https://www.ti.com/lit/an/slva372d/slva372d.pdf, accessed on May 2025.
[17] Teodorescu, R., Liserre, M., Rodríguez, P. (2011). Grid Converters for Photovoltaic and Wind Power Systems. Wiley-IEEE Press. https://doi.org/10.1002/9780470667057
[18] International Electrotechnical Commission, IEC 61853-1:2011, Photovoltaic (PV) Module Performance Testing and Energy Rating, Jan. 2011. https://webstore.iec.ch/en/publication/6035.
[19] Zerzouri, N., Ben Si Ali, N., Benalia, N. (2023). Maximum power point tracking of a photovoltaic system connected to a three-phase grid using variable step-size perturb and observe algorithm. Electrical Engineering & Electromechanics, (5): 37-46. https://doi.org/10.20998/2074-272X.2023.5.06
[20] Hadjidj, N., Benbrahim, M., Ounnas, D., Mouss, L. (2025). Global maximum power point tracking method for photovoltaic systems using Takagi-Sugeno fuzzy models and ANFIS approach. Electrical Engineering & Electromechanics, (2): 31-38. https://doi.org/10.20998/2074-272X.2025.2.05
[21] Ali, A., Mohamed, H. (2022). Improved P&O MPPT algorithm with efficient open-circuit voltage estimation for grid-integrated PV system under realistic solar radiation. International Journal of Electrical Power & Energy Systems, 137: 107805. https://doi.org/10.1016/j.ijepes.2021.107805
[22] Ali, A.I.M., Mousa, H.H., Mohamed, H.R.A., Kamel, S., Hassan, A.S., Alaas, Z.M. et al. (2023). An enhanced P&O MPPT algorithm with concise search area for grid-tied PV systems. IEEE Access, 11: 79408-79421. https://doi.org/10.1109/ACCESS.2023.3298106
[23] Erickson, R., Maksimović, D. (2020). Fundamentals of Power Electronics (3rd ed.). Springer. https://doi.org/10.1007/978-3-030-43881-4
[24] Saied, B., Mohammed, H. (2012). Voltage and frequency regulation of a three-phase induction generator using voltage source inverter. Al-Rafidain Engineering Journal, 20(1): 58-69. https://doi.org/10.33899/rengj.2012.47240
[25] Sabry, S., Enjeti, P. (2020). High frequency integrated solid-state transformer for utility interface of solar PV/battery energy storage systems. In Proceedings of the IEEE Applied Power Electronics Conference (APEC), New Orleans, LA, USA, pp. 546-553. https://doi.org/10.1109/APEC39645.2020.9124199
[26] Boyra, M., Thomas, J.L. (2011). A review on synchronization methods for grid-connected three-phase VSC under unbalanced and distorted conditions. In Proceedings of the 2011 14th European Conference on Power Electronics and Applications, Birmingham, UK, pp. 1-10.
[27] Zhao, J., Huang, M., Yan, H., Tse, C., Zha, X. (2021). Nonlinear and transient stability analysis of phase-locked loops in grid-connected converters. IEEE Transactions on Power Electronics, 36(1): 1018-1029. https://doi.org/10.1109/TPEL.2020.3000516
[28] Zou, Z., Besheli, B., Rosso, R., Liserre, M. (2019). Interactions between phase-locked loop synchronized grid converters with different bandwidths and power ratings. In Proceedings of the IEEE Energy Conversion Congress and Exposition, Baltimore, MD, USA, pp. 5430-5437. https://doi.org/10.1109/ECCE.2019.8912303
[29] Ke, S., Li, Y. (2023). Grid-connected phase-locked loop technology based on cascade second-order IIR filter. Energies, 16(9): 3967. https://doi.org/10.3390/en16093967
[30] Huang, L., Xin, H., Dong, W., Dörfler, F. (2022). Impacts of grid structure on PLL synchronization stability of converter-integrated power systems. IFAC-PapersOnLine, 55(13): 264-269. https://doi.org/10.1016/j.ifacol.2022.07.270
[31] Krause, P., Wasynczuk, O., Sudhoff, S., Pekarek, S. (2013). Analysis of Electric Machinery and Drive Systems (3rd ed.). Wiley.

https://doi.org/10.1002/9781118524336
[32] Ponomarev, A., Hagenmeyer, V., Gröll, L. (2024). Nonlinear analysis of the synchronous reference frame phase-locked loop under unbalanced grid voltage. Nonlinear Dynamics, 112: 9225-9243. https://doi.org/10.1007/s11071-024-09532-9
[33] Waqas, M., Ahmed, T., Elavarasan, R.M., Waqar, A. et al. (2021). DQ transformation based control of single-phase grid-tied inverter. In Proceedings of the Australasian Universities Power Engineering Conference, Perth, Australia, pp. 1-6. https://doi.org/10.1109/AUPEC52110.2021.9597712
[34] Ghasemi, M., Zarei, S., Peyghami, S., Blaabjerg, F. (2021). Theoretical concept of decoupled current control scheme for grid-connected inverter with LCL filter. Applied Sciences, 11(14): 6256. https://doi.org/10.3390/app11146256
[35] Temiz, H., Aydin, E., Yilmaz, A. (2019). Performance comparison of passive series-R and shunt RC damped LCL filter for grid-connected inverters. Journal of Engineering, 2019(18): 5221-5225. https://doi.org/10.1049/joe.2018.9321
[36] IEEE Standards Association. (2022). IEEE standard for harmonic control in electric power systems. IEEE Std 519-2022. https://doi.org/10.1109/IEEESTD.2022.9848440